Automatic Lung Segmentation with Seed Generation and ROIFT Algorithm for the Creation of Anatomical Atlas

Jungeui Choi[1], Edson K. Ueda[1], Guilherme C. Duran[1], Paulo A. V. Miranda[2], and Marcos S. G. Tsuzuki[1]

[1] Computational Geometry Laboratory, Escola Politécnica da USP, São Paulo, Brazil
[2] Instituto de Matemática e Estatística da USP, São Paulo, Brazil

Abstract. This paper describes the development of an algorithm to automatically generate seeds for lung CT (Computed Tomography) segmentation. The segmentation algorithm used is ROIFT (Relaxed Oriented Image Foresting Transform), a seed-based method for segmenting 3D images. Internal and external seeds are required for ROIFT. The internal and external seeds are automatically generated using the 2D watershed segmentation algorithm. Segmented images are transformed into a polyhedral model using the marching cubes algorithm. The segmented lungs will be used to create an anatomical atlas of the thoracic region. In this initial phase, 100 DICOM images were segmented. The anatomical atlas will be used as a regularization to solve the electrical impedance tomography of the human chest. Future work considers the segmentation of the ribs, skin, airways, and heart.

Keywords: Three-dimensional mesh · Anatomical atlas · Seed generation · Thoracic CT images · Watershed · Relaxed oriented image foresting transform.

1 Introduction

The image segmentation is very useful for medical and biological image analysis. However, to ensure reliable and accurate results, human supervision is necessary in several tasks, such as the extraction of poorly defined structures in medical imaging [4, 5, 17]. These problems have motivated the development of many semi-automatic segmentation methods with the aim of minimizing user involvement and time required without compromising accuracy. Some authors used temporal coherence to reduce user interaction [18, 21, 22, 24, 23]. In this research, segmentation will be performed automatically using an algorithm for automatic seed generation.

An important class of interactive image segmentation comprises seed-based methods, which were developed based on different, supposedly unrelated theories, such as Watershed [26] and Image Foresting Transform [3]. These methods can be used directly for automatic targeting when seeds are found automatically.

Segmented images will be used to create an anatomical atlas to regularize the electrical impedance tomography (EIT) problem [15, 20, 12, 13]. This work is an initial step for the creation of the anatomical atlas. It addresses lung segmentation. However, similar algorithms are expected to be created for the ribs, airways, heart, and skin in the near future. EIT consists of a non-invasive technique to obtain images of the interior of a contour through the knowledge of information in the contour itself [9, 10, 13, 14]. The anatomical atlas will be used to regularize the EIT problem [15, 11].

This paper will focus on the development of a fully automatic lung segmentation algorithm. Internal and external seeds will be automatically generated and will be used as input to the 3D Relaxed Oriented Image Foresting Transform (ROIFT) [2] segmentation algorithm. Internal and external seeds are generated using a 2D watershed segmentation algorithm and considering some geometrical assumptions.

This work is structured as follows. Section 2 presents a brief introduction of some basic concepts, such as DICOM images, watershed, Marching Cubes (MC) algorithm, Image Foresting Transform algorithm, Oriented Image Foresting Transform algorithm, and Relaxed Oriented Image Foresting Transform algorithm. Section 3 presents the proposed methodology to automatically generate seeds to be inputted into the ROIFT algorithm. In Section 4 the results will be presented, as well as the discussions, and the conclusions and future works are drawn in Section 5.

2 Basic Concepts

In this section, some basic concepts are presented. Initially, the medical images used in this work are described, which are 3D CT DICOM images of the human chest freely available on the Internet. After that, the Watershed and MC algorithms will be explained in detail, which are necessary processes for the generation of seeds used for segmentation via ROIFT, explained at the end of this section.

2.1 Medical Images

DICOM (Digital Imaging and Communications in Medicine) is a set of standards for the management and transmission of medical information (medical imaging) in a digital format. The DICOM standard is widely used in CT, MRI, radiography, ultrasound, etc. In this work, images of the thoracic region of the human body obtained by CT will be used for segmentation. Fig. 1 shows an example of a CT scan, a slice of the human chest. It is a 2D image, but it is possible to obtain a sequence of 2D images, where each image is a slice that makes up a 3D image.

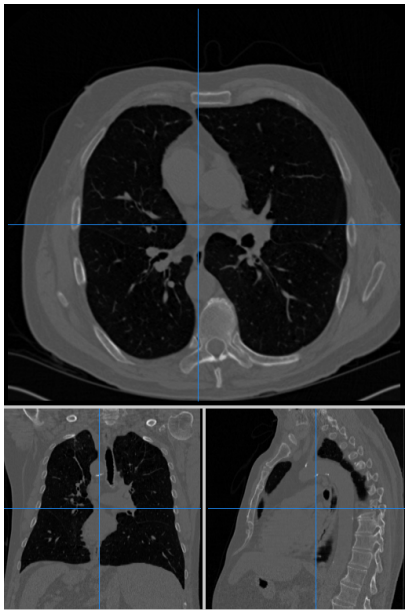

Fig. 1: Example of a CT DICOM image. It can be seen that the thoracic region is represented in three planes, a sagittal plane, a coronal plane and a transverse plane.

2.2 Watershed and Marching Cubes Algorithm

Watershed is an Image Segmentation Algorithm to detect basins in images [26]. The DICOM image is represented in shades of gray, and every grayscale image can be considered a topographic surface according to the watershed segmentation algorithm. The image is divided into two different sets: the catchment basin and the basin line, by filling the water surface with its minimum value and preventing the water from joining other sources. The Marching Cubes Algorithm [1, 25] computes a triangular mesh from discrete sample volume data and uses a divide-and-conquer approach to determine the isosurface inside a cubic cell. The vertices of the cell are classified as internal or external, with $2^8 = 256$ possible configurations for each cell.

Thus, the Watershed algorithm is used to segment each slice of the DICOM image, and all segmented images are converted into a 3D mesh STL (STereoLithography) file with the Marching Cubes algorithm. It was possible to segment the organs separately once each assumed a different grayscale value. Figs. 2(a), (b) and (c) represent, respectively, a rasterized representation of the lung, ribs, and airways that have been segmented from a CT image sequence.

It is important to note that, using the watershed algorithm, it was not possible to segment the heart and skin. In addition, there were several problems related to noise in bone segmentation, in addition to airway failures. Another

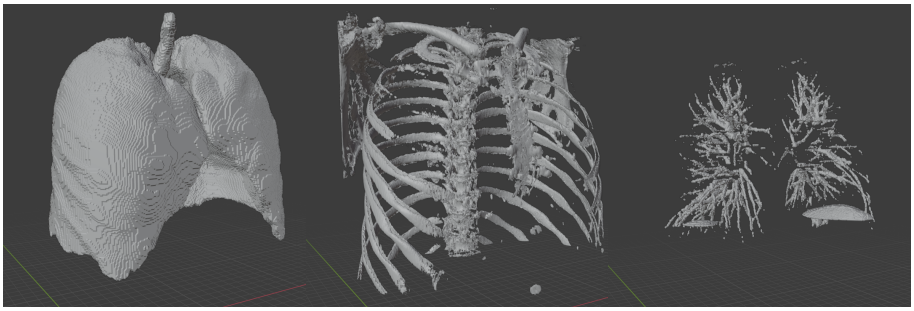

(a) (b) (c)

Fig. 2: (a) Lung. (b) Rib. (c) Airways.

problem of this approach is that continuity of the structures cannot be ensured between the slices, as noticed in Fig. 2(b), in which parts of the ribs are not correctly segmented.

2.3 IFT and OIFT

The Image Foresting Transform (IFT) [3] is an algorithm used in the development of image processing operators, with filtering, segmentation, and form representation, in which an image is transformed into a graph and the graph into a forest of optimal paths (minimum cost path forest)

The concept of a derivated image graph is used directly or indirectly in a lot of different techniques of image analysis, which, although they have similar concepts, are presented as unrelated methods, leading to different frameworks, such as watershed, random walk, fuzzy connectedness, and graph cuts. Depending on the framework used, the arc weights between a pixel of the graph can be interpreted as a similarity measure, velocity function, affinity, cost, or distance. The IFT unifies and extends many of these techniques by making use of more general search and connectivity optimization.

A multidimensional and multispectral image $\hat{I}$ is a pair $\langle \mathcal{I}, I \rangle$ where $\mathcal{I} \subset \mathrm{Z}^n$ is the image domain and $I(t)$ assigns a set of m scalars $I_i(t), i = 1, 2, ..., m$ to each pixel $t \in \mathcal{I}$. For a given image $\hat{I} = \langle \mathcal{I}, I \rangle$, an adjacency relation in $\mathcal{I}$ defines a directed graph $G = \langle \mathcal{V}, \mathcal{A}, \omega \rangle$ derivated in the image $\hat{I}$. Thus, in IFT a 2D/3D image can be interpreted as a directed graph G, in which the vertices $\mathcal{V}$ are the pixels/voxels of the image in its domain $\mathcal{I} \subset \mathrm{Z}^n$, the arcs are the ordered pairs of pixels $\langle s, t \rangle \in \mathcal{A} \subset \mathcal{I} \times \mathcal{I}$ and each arc $\langle s, t \rangle \in \mathcal{A}$ has an associated weight $\omega(\langle s, t \rangle) \geq 0$, which can be given by a dissimilarity measure between the pixels s and t, as well as each vertex $\mathcal{V} \in \mathcal{I}$ may have an associated weight $\omega(t) = \omega_v(t) \geq 0$. The set of adjacent nodes to s is denoted by $\mathcal{N}(s) = \{t \in \mathcal{V} : \langle s, t \rangle \in \mathcal{A}\}$.

The Oriented Image Foresting Transform (OIFT) [16, 7] is built on a dual version of the IFT framework considering that the arc weights ω_{st} represent a

directed affinity function, given by the power of complement of a combination of an undirected dissimilarity function κ_{st} between neighboring pixels s and t, multiplied by an orientation factor as

$$\omega_{st} = \begin{cases} [K - \kappa_{st} \times (1+\alpha)]^{\beta}, & \text{if } I(s) > I(t) \\ [K - \kappa_{st} \times (1-\alpha)]^{\beta}, & \text{if } I(s) < I(t) \\ [K - \kappa_{st}]^{\beta} & \text{otherwise .} \end{cases} \quad (1)$$

such that $\alpha \in [-1, 1]$ and K is the maximum weight value used for the complement calculation. Different procedures can be adopted for κ_{st}, such as using the absolute value of the difference in the intensities of the image (that is, $\kappa_{st} = |I(t) - I(s)|$). With $\alpha > 0$, the OIFT segmentation favors transitions from light to dark pixels and for $\alpha < 0$ favors the opposite orientation. The parameter $\beta > 0$ does not affect OIFT, but will be important for the ROIFT component.

2.4 Relaxed OIFT

The ROIFT algorithm [2] is a hybrid method between the OIFT and the Random Walks (RW) extension for directed graphs [19], producing segmentation results in more smooth and intuitive ways. As proposed by Demario and Miranda [2], extending the work of Malmberg et al. [6], for an initial computed segmentation $\mathcal{L}^0$, a sequence of fuzzy segmentations $\mathcal{L}^1, \mathcal{L}^1, ..., \mathcal{L}^N$ by iterative relaxation is obtained, as

$$\mathcal{L}^{i+1}(s) = \begin{cases} \frac{\sum_{t \in \mathcal{N}(s)} W^i(s,t) \cdot \mathcal{L}^i(t)}{\sum_{t \in \mathcal{N}(s)} W^i(s,t)}, & \text{if } s \notin \mathcal{S}_o \cup \mathcal{S}_b \\ \mathcal{L}^i(s) & \text{otherwise} \end{cases} \quad (2)$$

$$W^i(s,t) = \begin{cases} [K - \kappa_{st}]^{\beta} & \text{if } \mathcal{L}^i(s) = \mathcal{L}^i(t) \\ \omega_{st} & \text{if } \mathcal{L}^i(s) > \mathcal{L}^i(t) \\ \omega_{ts} & \text{if } \mathcal{L}^i(s) < \mathcal{L}^i(t) \end{cases} \quad (3)$$

such that $\mathcal{S}_o \subset \mathcal{V}$ and $\mathcal{S}_b \subset \mathcal{V}$ are two seed sets, in object/background segmentation, respectively. The final crisp $\mathcal{L}$ is obtained, by assigning $\mathcal{L}(s) = 1$ to all $s \in \mathcal{V}$ with $\mathcal{L}^N(s) \geq 0.5$ and $\mathcal{L}(s) = 0$ otherwise. This solution converges to RW for sufficiently high values of N, but the idea here is to consider a lower amount of relaxation to get a hybrid result, so that N controls the smoothness of the segmentation boundary, thus improving the results in the presence of noise and weak edges.

3 Proposed Automatic Seed Generation Algorithm

In this section, seed segmentation is presented in a more intuitive and visual way, and then the algorithm methodology for use in lung segmentation will be presented.

3.1 Seed Generation

The IFT/OIFT algorithm is initialized from background and object seeds. We can see in Fig. 3, that through the seeds, the algorithm searches for regions of the image that belong to the same object as the specified seed. For example, if the algorithm receives a seed of the background in an iteration, it will travel around the surroundings of that seed, guiding itself through similar regions to classify them as also being regions belonging to the background of the image.

(a) (b)

Fig. 3: (a) An image with two seed sets (markers), where the internal seed set $\mathcal{S}_o = \{r_1, r_2\}$ (internal markers) represents the object and the external seed set $\mathcal{S}_b = \{r_3, r_4\}$ (external markers) represents the background. (b) The segmentation result showing two forests of optimal paths rooted in the inner and outer seeds identifying the object and background respectively. The figure was taken from [8].

3.2 Algorithms for Seed Generation

Python libraries Numpy and Numpy-stl were used to develop the algorithm, which is useful for manipulating arrays and meshes. The seeds are represented as a list of three numbers that indicate the coordinates on the x, y, and z axes. The outer seeds are located in the center and on the side of the lung, while the internal seeds were determined as a set of seeds that form a sphere to obtain better segmentation accuracy, as shown in Fig. 4.

Initially, it is important to point out that the STL mesh resulting from the watershed algorithm returns inverted on the z-axis, which can bring seeds of wrong coordinates. In this way, the lung rotated 180^o with respect to the z-axis of origin and shifted to its original position. The hypothesis that the center of mass of the lung is on its external side is considered to calculate the coordinates of the first external seed. Therefore, the first outer seed (seed 1) was determined by calculating the center mass of the mesh, as shown in the line 4 of the simplified algorithm below. with the addition of a constant C to move the seed downwards,

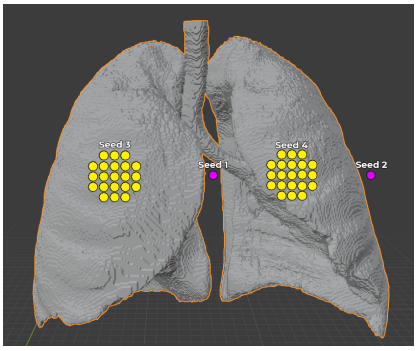

Fig. 4: The relative position of the seeds in the lung. The yellow dots represent the set of internal seeds (seeds 3 and 4), while the external ones (seeds 1 and 2) are represented by pink dot.

as some unexpected events may occur, such as having the seed inside the lung. The second outer seed (seed 2) was then found by calculating the value on the x axis of the side of the lung, a constant so that it is not so far from the lung (line 8). For the values y and z, the center-of-mass values were reused.

The center of mass calculation was also used for each lung to determine internal seeds (seeds 3 and 4). To split the lung, it was necessary to center it and then find the voxel coordinate closest to the origin to split it perfectly (line 7). After that, the single mesh was separated into two, they were returned to their original positions, and the seeds were calculated as the center of mass of both meshes (lines 9-12). Finally, to calculate the adjacent seeds, constant values were added until forming a seed sphere (lines 14-15).

Algorithm 1 Proposed methodology to determine the four seeds for the lung

```
1: Input: STL file
2: CenterOfGravity ← lung.getMassProperties()
3: Centralizes the STL using the current Center Of Gravity
4: Seed1[x, y, z - C] ← CenterOfGravity
5: Find the vectors (Three-dimensional array) from the lung
6: Divide the lung in two, using the vectors and the CenterOfGravity properties
7: rightlung, leftlung ← lung.divide()
8: Seed2[x, y, z] ← [rightlung.max(x)-C, rightlung.mean(y), rightlung.mean(z)]
9: RightCenterOfGravity ← rightlung.getMassProperties()
10: LeftCenterOfGravity ← leftlung.getMassProperties()
11: Seed3[x, y, z] ← RightCenterOfGravity
12: Seed4[x, y, z] ← LeftCenterOfGravity
13: for i in range(seedsinsphere):
14:     AdjSeeds3[x, y, z] ← Seed3[x+1, y+1, z+1] or Seed3[x-1, y-1, z-1]
15:     AdjSeeds4[x, y, z] ← Seed4[x+1, y+1, z+1] or Seed4[x-1, y-1, z-1]
16: return Seed1, Seed2, Seed3, Seed4, AdjSeeds3, AdjSeeds4
```

4 Results

A dataset of DICOM images of a total of 100 CT images of the human chest was used for segmentation, taken from the Data Science Bowl 2017 competition. Unfortunately, the data are currently not available for access. In these images, 6 were not possible for segmentation via the watershed. Thus, the seed generation algorithm only created seeds with viable coordinates in 94 images. Among all of them, the ROIFT algorithm was able to perfectly segment and convert to STL files. However, of the 94 images, 4 meshes had problems segmenting only one side of the lung, as shown in Fig. 5. The problem was due to the seed generation program, which will be corrected in future research.

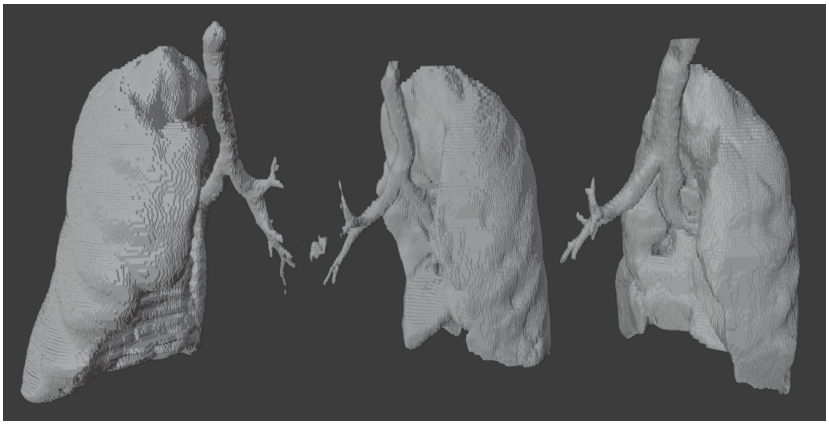

Fig. 5: Failed segmented meshes

Compared to the watershed, the ROIFT algorithm was superior in fundamental aspects: it was able to correct for noise that appeared in unexpected regions of the lung in the watershed, filing incomplete regions in the lower region of the lung, as shown in Fig. 6. ROIFT performed better in terms of processing time. However, if the size of the file is something to consider, you can increase the number of iterations of fuzzy segmentation, increasing the running time, and decreasing the file size. The table 1 shows the details of each procedure. Two ROIFT segmentations were performed, one with 5 iterations and another with 25, to show the difference in the file size and processing time of the segmentations. Visually, one might notice a difference in mesh smoothing, as shown in Fig. 7.

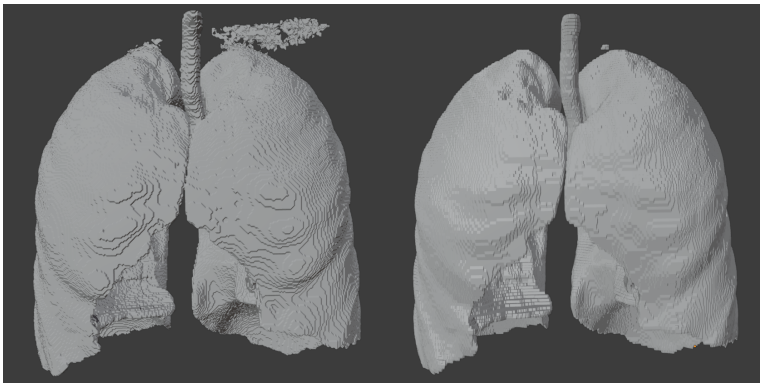

(a) (b)

Fig. 6: (a) Watershed lung segmentation. (b) ROIFT lung segmentation.

Table 1: Algorithm comparison in 100 DICOM images. SA = Segmentation Algorithm. ROIFT 5 it = ROIFT with 5 iterations. ROIFT 25 it = ROIFT with 25 iterations. RT = running time. The accuracy represents the value in percentage of correctly segmented lungs divided by the total segmented images.

SA	RT	File size	Accuracy
Watershed	3,893.56 s	7.1 GB	94%
ROIFT 5 it	2,990.52 s	5.5 GB	96%
ROIFT 25 it	5,298.75 s	4.8 GB	96%

5 Conclusions and Future Work

In this work, we developed algorithms for automatic seed generation and used the ROIFT algorithm to segment the lungs in the thorax region. The method used in this paper showed better results in terms of segmentation time and noise reduction compared to the watershed segmentation algorithm.

Automatic seed generation methods are in the process of being developed for the rib and for the skin. When testing with seeds manually, ROIFT has already presented significant results. Fig.8 shows the differences between the two rib segmentation methods. Skin segmentation was not possible using the watershed. However, it is feasible to use ROIFT for the procedure, as shown in Fig.9.

Other regions of the chest will still be automatically segmented via ROIFT, such as: ribs, airways, skin, and heart. In this way, alternative ways of generating seeds will be developed.

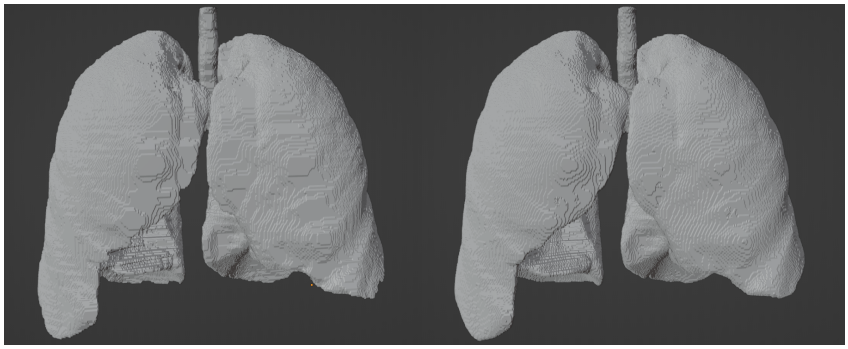

(a) (b)

Fig. 7: (a) Segmentation with 5 iterations. (b) Segmentation with 25 iterations.

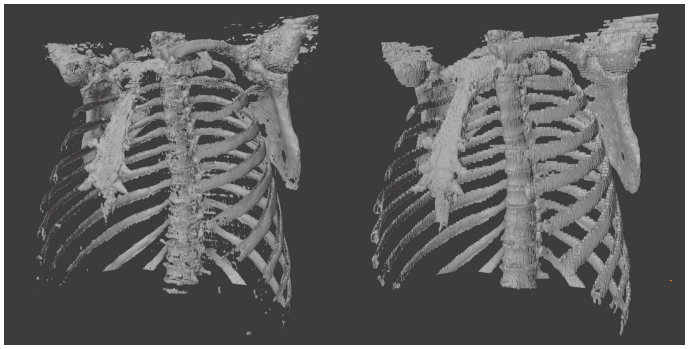

(a) (b)

Fig. 8: (a) Watershed rib segmentation. (b) ROIFT rib segmentation.

References

1. Chernyaev, E.V.: Marching cubes 33: Construction of topologically correct isosurfaces. Tech. rep. (1995)
2. Demario, C.L., Miranda, P.A.V.: Relaxed oriented image foresting transform for seeded image segmentation. In: IEEE ICIP. pp. 1520–1524 (2019)
3. Falcao, A., Stolfi, J., de Alencar Lotufo, R.: The image foresting transform: theory, algorithms, and applications. IEEE T Pattern Anal **26**(1), 19–29 (2004)
4. Iwao, Y., Gotoh, T., Kagei, S., Iwasawa, T., Tsuzuki, M.S.G.: Integrated lung field segmentation of injured regions and anatomical structures from chest CT images. IFAC Proceedings Volumes (IFAC-PapersOnline) **45**, 85–90 (2012)
5. Iwao, Y., Gotoh, T., Kagei, S., Iwasawa, T., Tsuzuki, M.S.G.: Integrated lung field segmentation of injured region with anatomical structure analysis by failure-recovery algorithm from chest CT images. Biomed Signal Proces **12**, 28–38 (2014)

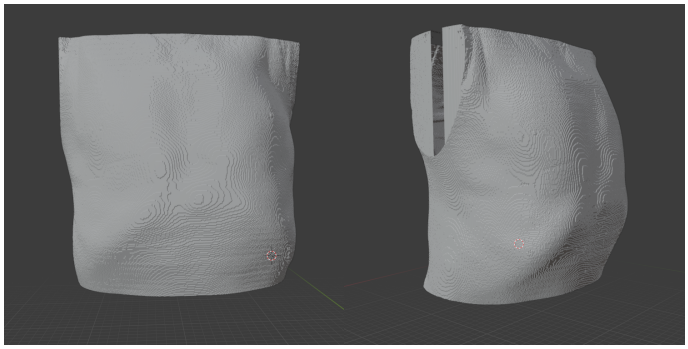

(a) (b)

Fig. 9: (a) Front view of skin segmentation. (b) Side and rear representation of skin.

6. Malmberg, F., Nyström, I., Mehnert, A., Engstrom, C., Bengtsson, E.: Relaxed image foresting transforms for interactive volume image segmentation. In: Proc SPIE: Progress in Biomedical Optics and Imaging. vol. 7623, pp. 1–11. SPIE, United States (2010)
7. Mansilla, L.A.C., Miranda, P.A.: Image segmentation by oriented image foresting transform: Handling ties and colored images. In: 18th Int Conf DSP. pp. 1–6 (2013)
8. Mansilla, L.A.C.: Segmentação de Objetos via Transformada Imagem-Floresta Orientada com Restrições de Conexidade. Ph.D. thesis, Instituto de Matemática e Estatística da USP, São Paulo, Brasil (2018)
9. Martins, T.C., Tsuzuki, M.S.G.: Simulated annealing with partial evaluation of objective function applied to electrical impedance tomography. IFAC Proceedings Volumes **44**(1), 4989–4994 (2011), 18th IFAC WC
10. Martins, T.C., Tsuzuki, M.S.G.: Electrical impedance tomography reconstruction through simulated annealing with total least square error as objective function. In: 34th IEEE EMBC. pp. 1518–1521. San Diego, USA (2012)
11. Martins, T.C., Tsuzuki, M.S.G.: Electrical impedance tomography reconstruction through simulated annealing with multi-stage partially evaluated objective functions. In: 35th IEEE EMBC. pp. 6425–6428 (2013)
12. Martins, T.C., Tsuzuki, M.S.G.: Investigating anisotropic EIT with simulated annealing. IFAC-PapersOnLine **50**(1), 9961–9966 (2017), 20th IFAC WC
13. Martins, T.C., Tsuzuki, M.S.G.: EIT image regularization by a new multi-objective simulated annealing algorithm. In: 37th IEEE EMBC. pp. 4069–4072. Milan, Italy (2015)
14. Martins, T.C., Fernandes, A.V., Tsuzuki, M.S.G.: Image reconstruction by electrical impedance tomography using multi-objective simulated annealing. In: 11th IEEE ISBI. pp. 185–188. Beijing, China (2014)
15. Martins, T.C., Sato, A.K., de Moura, F.S., de Camargo, E.D.L.B., Silva, O.L., Santos, T.B.R., Zhao, Z., Möeller, K., Amato, M.B.P., Mueller, J.L., Lima, R.G., Tsuzuki, M.S.G.: A review of electrical impedance tomography in lung applications: Theory and algorithms for absolute images. Annu Rev Control **48**, 442–471 (2019)

16. Miranda, P.A.V., Mansilla, L.A.C.: Oriented image foresting transform segmentation by seed competition. IEEE T Image Process **23**(1), 389–398 (2014)
17. Olabarriaga, S.D., Smeulders, A.W.: Interaction in the segmentation of medical images: a survey. Med Image Anal **5**(2), 127–142 (jun 2001)
18. Sato, A.K., Stevo, N.A., Tavares, R.S., Tsuzuki, M.S.G., Kadota, E., Gotoh, T., Kagei, S., Iwasawa, T.: Registration of temporal sequences of coronal and sagittal MR images through respiratory patterns. Biomed Signal Proces **6**, 34–47 (2011)
19. Singaraju, D., Grady, L., Vidal, R.: Interactive image segmentation via minimization of quadratic energies on directed graphs. In: Intl. Conf. CVPR. pp. 1–8 (2008)
20. Tavares, R.S., Martins, T.C., Tsuzuki, M.S.G.: Electrical impedance tomography reconstruction through simulated annealing using a new outside-in heuristic and GPU parallelization. J Phys Conf Ser **407**, 012015 (dec 2012)
21. Tavares, R.S., Chirinos, J.M.M., Abe, L.I., Gotoh, T., Kagei, S., Iwasawa, T., Tsuzuki, M.S.G.: Temporal segmentation of lung region from MRI sequences using multiple active contours. In: 32nd IEEE EMBC. pp. 7985–7988. Buenos Aires, Argentina (2011)
22. Tavares, R.S., Sato, A.K., Tsuzuki, M.S.G., Gotoh, T., Kagei, S., Iwasawa, T.: Temporal segmentation of lung region MR image sequences using Hough transform. In: 32nd IEEE EMBC. pp. 4789–4792. Buenos Aires, Argentina (2010)
23. Tavares, R.S., Tsuzuki, M.S.G., Gotoh, T., Kagei, S., Iwasawa, T.: Lung movement determination in temporal sequences of MR images using hough transform and interval arithmetics. In: Proc 7th IFAC Symposium on Modelling and Control in Biomedical Systems. pp. 192–197. Alborg, Denmark (2009)
24. Tsuzuki, M.S.G., Takase, F.K., Gotoh, T., Kagei, S., Asakura, A., Iwasawa, T., Inoue, T.: Animated solid model of the lung constructed from unsynchronized MR sequential images. CAD **41**, 573–585 (8 2009)
25. Tsuzuki, M.S.G., Sato, A.K., Ueda, E.K., Martins, T.C., Takimoto, R.Y., Iwao, Y., Abe, L.I., Gotoh, T., Kagei, S.: Propagation-based marching cubes algorithm using open boundary loop. Vis Comput **34**(10), 1339–1355 (oct 2018)
26. Vincent, L., Soille, P.: Watersheds in digital spaces: an efficient algorithm based on immersion simulations. IEEE T Pattern Anal **13**(6), 583–598 (1991)